

Low-Dimensional Gradient Helps Out-of-Distribution Detection

Yingwen Wu, Tao Li, Xinwen Cheng, Jie Yang *Senior Member, IEEE*, Xiaolin Huang *Senior Member, IEEE*

Abstract—Detecting out-of-distribution (OOD) samples is essential for ensuring the reliability of deep neural networks (DNNs) in real-world scenarios. While previous research has predominantly investigated the disparity between in-distribution (ID) and OOD data through forward information analysis, the discrepancy in parameter gradients during the backward process of DNNs has received insufficient attention. Existing studies on gradient disparities mainly focus on the utilization of gradient norms, neglecting the wealth of information embedded in gradient directions. To bridge this gap, in this paper, we conduct a comprehensive investigation into leveraging the entirety of gradient information for OOD detection. The primary challenge arises from the high dimensionality of gradients due to the large number of network parameters. To solve this problem, we propose performing linear dimension reduction on the gradient using a designated subspace that comprises principal components. This innovative technique enables us to obtain a low-dimensional representation of the gradient with minimal information loss. Subsequently, by integrating the reduced gradient with various existing detection score functions, our approach demonstrates superior performance across a wide range of detection tasks. For instance, on the ImageNet benchmark, our method achieves an average reduction of 11.15% in the false positive rate at 95% recall (FPR95) compared to the current state-of-the-art approach. The code would be released.

Index Terms—out-of-distribution detection, gradient dimension reduction, deep neural networks

I. INTRODUCTION

IN an open-world setting, a reliable system should not only provide accurate predictions but also issue appropriate warnings when it encounters unknown data. Consequently, a field worthy of research called out-of-distribution (OOD) detection has emerged with the rapid development of deep neural networks (DNNs). Typically, DNNs are assumed to be trained and tested on datasets drawn from the same distribution. This assumption enables DNNs to generate precise predictions on test data, which is called in-distribution (ID) data. However, in open-world scenarios, this assumption can be easily invalidated. For instance, in autonomous driving, it is infeasible for the training dataset to encompass all potential scenarios. Therefore, the presence of OOD inputs necessitates the ability to recognize them for a reliable DNN. In this regard, the algorithm for OOD detection holds substantial practical significance.

A rich line of research has been developed for OOD detection. For instance, output-based methods have revealed that the prediction confidence of ID data is generally higher

than that of OOD data [1]–[3]. Consequently, multiple score functions have been devised based on model outputs. Besides, several studies have investigated the disparities in intermediate features between ID and OOD data [4]–[7]. These studies have observed that features of ID data tend to cluster together and differ significantly from those of OOD data. Building upon this observation, various score functions, such as Maha [6] and KNN [7], have been proposed for OOD detection.

All the aforementioned methods utilize forward information, *i.e.*, information generated in the forward process, to detect OOD inputs. However, it is important to note that the disparities between ID and OOD data are also significant in the backward process of DNNs [8]–[13]. For instance, the parameter gradient magnitude for ID data is expected to be generally smaller than that of OOD data, considering the well-trained nature of DNNs on ID data. This observation has spurred several intriguing OOD detection methods, such as GradNorm [9], which capitalizes on the gradient norm as its score function. However, a comprehensive investigation into the divergence of parameter gradients between ID and OOD data is still lacking. The primary challenge arises from the fact that the parameter gradient, representing the backward information, exists in a high-dimensional space for modern DNNs. Consequently, distance measurements within this space exhibit inherent unreliability due to a well-known phenomenon called the dimension curse [14]. This phenomenon refers to the tendency for distances between data points to become increasingly similar as the number of dimensions increases, thereby rendering the distinction between ID and OOD data difficult to discern in their high-dimensional gradient space.

To tackle the essential difficulty raised by high dimensionality, we propose to perform dimension reduction on the gradient. Admittedly, dimension reduction involves the potential loss of crucial information associated with significant dimensions, which may undermine its efficacy in OOD detection. Nevertheless, recent studies indicate that the gradient of ID data may mainly fall into a relatively low-dimensional space. The related theoretical discussions and empirical evaluations include:

- Subspace training [15]: During the training process, the gradient of network parameters falls into a data-dependent, low-dimensional subspace;
- Low-rank adaptation [16]: The change of network parameters for a fine-tuning task is a low-rank adaptation matrix;
- Low-rank spectrum of neural tangent kernel [17]–[19]: The neural tangent kernel matrix, consisting of gradient inner products, has a low-rank spectrum.

Y. Wu, T. Li, X. Cheng and X. Huang are with the Department of Automation, Shanghai Jiao Tong University, 200240 Shanghai, P.R. China. Email: {yingwen_wu, li.tao, xinwencheng, xiaolinhuang}@sjtu.edu.cn

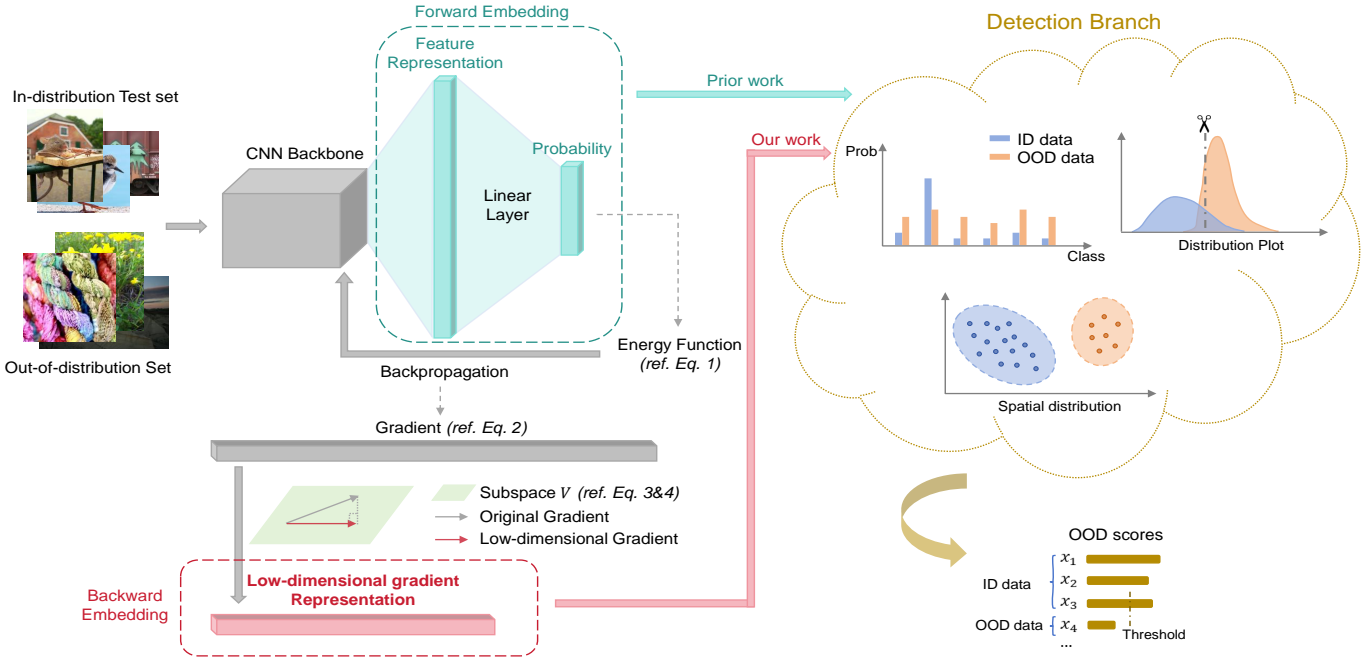


Fig. 1. **Illustration of our framework using low-dimensional gradients for OOD detection.** Firstly, we obtain the parameter gradients of inputs from a complete backpropagation process of our model. Then, using a pre-extracted subspace where the principal components of training data gradients reside, we obtain low-dimensional representations through a projection operation. Finally, we feed the representations into the detection branch, where diverse score functions are designed based on these representations.

Table I. Simple modifications and superior performance when our low-dimensional gradients are integrated with six baseline methods. We report the FPR95 and AUROC metrics of our approach on the ImageNet benchmark. The comparison results with baseline methods are presented in brackets, where the green color indicates that our method outperforms the baseline. The symbol \uparrow denotes that larger values are better and vice versa.

Method	Type	Simple Modification	FPR95 \downarrow	AUROC \uparrow
MSP [1]	Output-based	An additional linear network	32.28 (\downarrow 32.38)	91.87 (\uparrow 9.05)
Energy [2]	Output-based	An additional linear network	27.90 (\downarrow 29.57)	93.09 (\uparrow 6.04)
ReAct [4]	Feature-based	Adaptive threshold	23.03 (\downarrow 7.67)	95.45 (\uparrow 2.15)
BTAS [5]	Feature-based	Adaptive threshold	23.42 (\downarrow 34.13)	95.40 (\uparrow 8.36)
Maha [6]	Feature-based	None	87.30 (\uparrow 5.79)	49.31 (\downarrow 14.78)
KNN [7]	Feature-based	None	41.18 (\downarrow 15.12)	88.10 (\uparrow 2.84)
Ensemble	-	-	19.55 (\downarrow 11.15)	96.12 (\uparrow 2.82)

These discussions shed light on an important insight: parameter gradients lie in a relatively low-dimensional space, offering the possibility of linear dimension reduction while preserving significant information for effective OOD detection. The key problem now revolves around identifying the subspace where the principal components of gradients reside. One approach we use comes from NFK [20], which employs an efficient algorithm to compute the top eigenvectors of a gradient covariance matrix. However, this method incurs notable computational costs due to the high dimensionality of gradients. To mitigate the computational burden, we also propose an alternative method to estimate the subspace. Building on the observation that gradients of samples belonging to the same class exhibit a pronounced degree of direction similarity [18], [21], we propose using the average gradient of each class as the basis for the subspace. This approach is easier to implement but retains less information within its subspace compared to the first one. In practical applications, users

can flexibly choose the above two approaches based on data volume and model size. Once the subspace is determined, the gradients can be projected onto it, yielding low-dimensional representations. These representations can then be effectively utilized to discriminate between ID and OOD samples.

Given that the reduced gradients serve as a distinctive form of data representation [13], [22], the approaches that use forward embeddings can be seamlessly integrated with our reduced gradients. The possible choices include MSP [1] and Energy [2], which utilize output differences; ReAct [4] and BATS [5], which employ feature distribution differences; and Mahalanobis [6] and KNN [7], which use pairwise information. With simple modifications to these approaches (see Table I), our reduced gradients can be effectively combined with them and show remarkable improvements in detection performance. Additionally, we discover that an ensemble of forward and backward information can further improve our detection performance since data samples exhibiting minimal

disparities in the forward features may exhibit substantial variations in the backward gradients.

The overall framework of our method is illustrated in Figure 1. To evaluate its effectiveness, we conduct experiments on two widely used benchmark datasets: CIFAR10 [23] and ImageNet [24], along with seven OOD datasets. We evaluate the performance of the above-mentioned six methods based on forward features and backward gradients respectively. The experimental results demonstrate the superior performance of our low-dimensional gradients on both benchmark datasets, see Table I. Notably, on the large-scale ImageNet benchmark, our method outperforms the best baseline by 11.15% in terms of False Positive Rate at 95% True Positive Rate (FPR95), and by 2.82% in terms of Area Under the Receiver Operating Characteristic Curve (AUROC). The contributions of this paper can be summarized as follows:

- We present a pioneering investigation into the utilization of complete gradient information for OOD detection, offering novel insights into this field.
- Our proposed gradient dimension reduction algorithm offers a valuable technical contribution, providing a solid foundation for future studies on leveraging gradients in OOD detection.
- We demonstrate the remarkable performance of our low-dimensional gradients across a diverse range of OOD detection tasks.

II. RELATED WORK

The existing OOD detection approaches can be categorized into three types: 1) density-based; 2) post-hoc; 3) confidence enhancement.

Density-based methods explicitly model the in-distribution data with some probabilistic models and flag test data in low-density regions as OOD data. For example, Mahalanobis [6] uses class-conditional Gaussian distribution to model the in-distribution data and detect OOD samples with their likelihoods. Flow-based methods [25]–[28] are also effective in probabilistic modeling for OOD detection. Besides, researchers also investigate the effect of an ensemble of multiple density models [29]. However, due to the difficulty of optimizing generative models, density-based methods are hardly used in practice.

Post-hoc methods are the most popular in OOD detection because of their portability and effectiveness. These approaches aim to design a score function that assigns high scores to ID data and low scores to OOD data, enabling the separation of OOD samples by applying an appropriate threshold. Based on the way of calculating scores, these methods can be broadly divided into three types: 1) output-based; 2) feature-based; and 3) gradient-based. Classical output-based methods, such as MSP [1], ODIN [3], and Energy [2], design score functions based on the observation that classification probabilities of OOD samples tend to be lower than those of normal data. In pursuit of enhanced detection performance, ReAct [4] and BATS [5] propose to truncate the abnormal values of intermediate features, thereby amplifying the disparities between ID

and OOD data in the output space. Feature-based approaches, as exemplified by KNN [7], Maha [6], and other related works [30], [31], primarily leverage the aggregation property of ID features to identify OOD samples. For instance, Maha [6] utilizes the Mahalanobis distance between the feature of inputs and the mean feature of corresponding classes as its score function for OOD detection. Similarly, KNN [7] employs the Euclidean distance to the k -th nearest neighborhood as a measurement to detect OOD data. Furthermore, several studies [30], [31] leverage the inherent low-dimensional characteristics of features and introduce reconstruction errors as detection scores to identify OOD data. Gradient-based approaches, such as GradNorm [9], Purview [10], GraN [32], and others [8], [11], [12], mainly focus on utilizing the norm of parameter gradients to detect OOD samples. For instance, GradNorm [9] shows that the gradient norm calculated from the categorical cross-entropy loss is generally lower on OOD data, thereby designing detection functions based on the norm. Other studies employ the gradient norm in different ways, like introducing binary networks [12], etc [8], [10], [11], [32]. Apart from the above mentioned approaches, Vim [33] empirically demonstrates that a combination of output and feature information can further improve detection performance. Our proposed method also belongs to the post-hoc type, which is plug-and-play in practice.

Confidence enhancement methods design various regularization terms to amplify the difference between ID and OOD data. For example, models are encouraged to give uniformly distributed predictions [34]–[36] or higher energies [2], [37]–[39] on outlier data. Another type of regularization term is to apply contrastive losses such as SimCLR [40], SupCon [41], and Cider [42] to promote stronger ID-OOD separability. However, confidence enhancement methods typically require model retraining, and in some cases, even necessitate the acquisition of additional OOD data. These requirements render such methods impractical for real-world applications.

III. METHOD

A. Preliminary

The framework of OOD detection can be described as follows. We consider a classification problem with C classes, where \mathcal{X} stands for the input space and \mathcal{Y} for the label space. The joint data distribution over $\mathcal{X} \times \mathcal{Y}$ is denoted as $D_{\mathcal{X}\mathcal{Y}}$. Let $f_\theta : \mathcal{X} \mapsto \mathcal{Y}$ be a model trained on samples drawn *i.i.d.* from $D_{\mathcal{X}\mathcal{Y}}$ with parameter θ . Then the distribution of ID data is denoted as D_{in} , which is the marginal distribution of $D_{\mathcal{X}\mathcal{Y}}$ over \mathcal{X} . The distribution of OOD data is presented as D_{out} , whose label set has no intersection with \mathcal{Y} . The goal of OOD detection is to decide whether a test input x is from D_{in} or D_{out} . For post-hoc methods, the decision is made through a score function S as follows:

$$G_\lambda(x) = \begin{cases} \text{ID} & \text{if } S(x, f) \geq \lambda, \\ \text{OOD} & \text{if } S(x, f) < \lambda, \end{cases}$$

where λ is a threshold and samples with scores higher than λ are classified as ID data. The threshold is usually set based

on ID data to guarantee that a high fraction of ID data (e.g. 95%) is correctly identified as ID samples.

B. Low-dimensional Gradient Extraction

In this section, we progressively answer two questions: 1) how to calculate gradients in the label-agnostic condition? 2) how to reduce the gradient dimension and simultaneously retain as much information as possible? In the context of OOD detection, input labels are inaccessible to users, and thus the normal cross-entropy loss used in the training process is not applicable to calculating gradients for test data. Borrowing the idea from JEM [43], we induce a label-free energy function that has the same conditional probability $p_\theta(y|x) = \exp(f_\theta^y(x)) / \sum_y \exp(f_\theta^y(x))$ as the original model:

$$E(x; \theta) = -\log \sum_y \exp(f_\theta^y(x)) \quad (1)$$

It essentially reframes a conditional distribution over y given x to an induced unconditional distribution over x . With the energy-based model $E(x; \theta)$, we can calculate the gradient given any input x without y as follows:

$$\nabla_\theta E(x; \theta) = -\sum_y p_\theta(y|x) \nabla_\theta f_\theta^y(x) \quad (2)$$

It is equivalent to a weighted average of the derivative of outputs for all labels. To eliminate the scale discrepancies among different dimensions, we normalize it using the mean and variance matrix calculated from the training data:

$$\mathcal{M} = \mathbb{E}_{x \sim D_{in}} \frac{\partial E(x; \theta)}{\partial \theta}, \quad \mathcal{I} = \mathbb{E}_{x \sim D_{in}} [U(x)U(x)^T]$$

$$G(x) = (\text{diag}(\mathcal{I})^{-\frac{1}{2}})(\nabla_\theta E(x; \theta) - \mathcal{M})$$

where \mathcal{M} and \mathcal{I} are the mean and variance matrix, and $G(x)$ is the normalized gradient of sample x . After obtaining the label-agnostic gradient, the next crucial problem is reducing its dimension to facilitate its practical utilization. Recent empirical studies, such as LoRA [16] and DLDR [15], have shown that the gradient of ID data reside in a low-dimensional subspace. The low-rank spectrum analysis [17]–[19] of neural tangent kernel (NTK, [44]) has also provided theoretical evidence explaining the above phenomenon. Therefore, a simple linear dimension reduction method is sufficient for extracting a low-dimensional representation of the gradient. The most commonly used algorithm is principal component analysis (PCA, [45]), which employs the top-K eigenvectors of the gradient covariance matrix as its dimension reduction matrix. Denote the eigen decomposition as follows:

$$C = V\Sigma V^T, \quad (3)$$

where C is the gradient covariance matrix computed on all the training data. Based on the diagonal values of Σ , PCA selects K column vectors of V corresponding to the first K large eigenvalues. Then the low-dimensional representation is calculated as follows:

$$G_{low} = GV.$$

Because of the high dimensionality of gradients, the above eigen decomposition cannot be calculated directly in practice.

Hence, we adopt a power iteration method [46], [47] to obtain the eigenvectors under reasonable computation costs, following the idea in NFK [20]. Specific algorithms are in Appendix A.

In addition to the PCA algorithm, in this paper, we also propose an alternative approach to estimate the low-dimensional subspace encompassing principal components. Drawing upon the observation that the parameter update induced by a sample has a more pronounced influence on samples belonging to the same class while exerting minimal influence on samples from other classes [48]–[50], it is reasonable to infer that parameter gradients from samples within the same class tend to align in similar directions. Previous empirical studies [18], [21] support the above inference by demonstrating that parameter gradients from samples of the same class exhibit a high degree of direction similarity. Moreover, our empirical experiments, detailed in Appendix B, further validate the above claim by revealing a high cosine similarity between the gradients of samples from the same class and their corresponding gradient centers. Based on these findings, we propose utilizing the average gradient of each class as an alternative subspace estimation:

$$V \triangleq \{\mathbb{E}_{(x,y) \sim D_{xy}} [G(x|y=c)]\}, \quad c = 1, 2, \dots, C. \quad (4)$$

In this way, the extraction of low-dimensional subspace becomes easy to implement. However, this subspace is not accurate, and the dimension depends on the number of classes C . Therefore, it is more suitable for scenarios involving large volumes of data and complex models, where the computation of principal components using PCA necessitates substantial computational resources.

Based on the above two subspace extraction methodologies, the overall algorithm for calculating the low-dimensional gradient is shown in Alg 1. It is worth-noticing that although the subspace extraction process takes some computing time, the follow-up projection process can be fast with efficient parallel calculation. Specifically, the subspace can be partitioned into multiple lower-dimensional subspaces, each of which can be stored on different GPUs. Then, the projection process can be independently executed on each GPU. By subsequently concatenating the outcomes obtained from each individual GPU, the final low-dimensional gradient can be obtained efficiently.

Algorithm 1 Low-dimensional Gradient Calculation

Input: model f_θ , sample x , mean \mathcal{M} , variance \mathcal{I}

Output: The low-dimensional gradient of x

- 1: Extract the principal subspace V using Eq (3) or Eq (4).
 - 2: $G_{org} \leftarrow (\text{diag}(\mathcal{I})^{-\frac{1}{2}})(-\sum_y p_\theta(y|x) \nabla_\theta f_\theta^y(x) - \mathcal{M})$
 - 3: $G_{low} \leftarrow G_{org}V$
 - 4: **return** G_{low}
-

C. Score Function Design

This section elucidates the application of low-dimensional gradients in OOD detection. To design effective score functions based on the gradients, we first analyze their properties

to figure out the divergence of them between ID and OOD data. The visualization of our low-dimensional gradients presented in Figure 2 reveals a discernible phenomenon: the low-dimensional gradients derived from ID data tend to exhibit clustering, forming cohesive groups, while simultaneously manifesting a distinctive separation from the gradients originating from OOD data. This observation demonstrates a striking parallel to the clustering and separation patterns observed in forward features. Therefore, prior distance-based methods such as Maha [6] and KNN [7] can be seamlessly adapted to operate on our gradients. Furthermore, since our gradients show the separability between samples of different classes, they can serve as a distinctive form of data representation and be used to classify samples. Thus, output-based methods [1], [2] can also be combined with our gradients. Apart from the visualization analysis, we also investigate the distribution of our gradients to dig up their distinctions between ID and OOD data. As Figure 3 shows, the values of OOD gradients fall within the range of ID gradients in the top- n dimensions (n is a number close to the number of classes C), while in the rest dimensions, their values are noticeably larger. Hence, we can employ previous feature rectification methods [4], [5] on the rest dimensions of our gradients to obtain improved detection performance compared to the output-based methods.



Fig. 2. Visualization of penultimate features (left) and low-dimensional gradients (right) via t-SNE [51]. The model is trained with ResNet18 on CIFAR10.

Subsequently, we provide detailed explanations regarding the integration of our gradients with output-based methods [1], [2], feature rectification methods [4], [5], and distance-based methods [6], [7]. Besides, inspired by the ensemble strategy proposed in Vim [52], we also explore a simple ensemble technique that combines forward and backward information to achieve enhanced OOD detection performance.

1) *Combination with output-based methods:* Output-based approaches aim to capture the dissimilarities in feature representations between ID and OOD data by modulating the network output using a linear layer. Consequently, we introduce an auxiliary linear network, trained on our reduced gradient, to generate the necessary output for computing score functions. The network architecture is:

$$g \rightarrow \text{BN} \rightarrow \text{FC} \rightarrow y \quad (5)$$

We adopt cross-entropy loss function and stochastic gradient descent (SGD) algorithm to train this network. The simplicity of our model enables a rapid training process. Once the linear network has been effectively trained, we can leverage its output

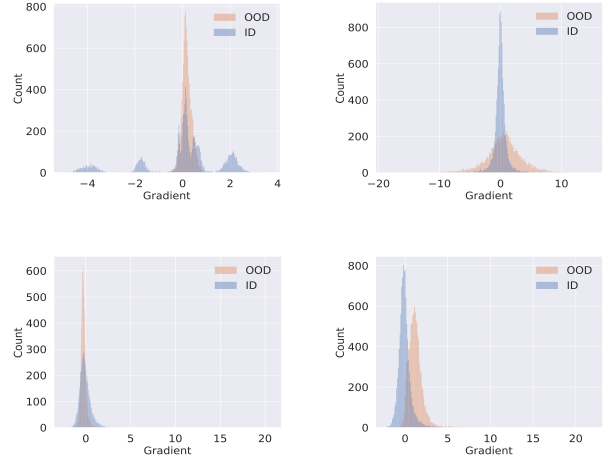


Fig. 3. The density distribution of our low-dimensional gradients on CIFAR10 and ImageNet on different dimensions. Top left: The 9-th dimension of our reduced gradient on CIFAR10. Top right: The 11-th dimension on CIFAR10. Bottom left: The 1-th dimension on ImageNet. Bottom right: The 999-th dimension on ImageNet. These plots reveal that the distribution differences between ID and OOD data is more distinguishable on the later dimensions.

to discriminate between ID and OOD samples. The basic score function is the maximum softmax confidence [1], *i.e.*,

$$S_1(x, f) = \max_j \frac{e^{y_j}}{\sum_j e^{y_j}}. \quad (6)$$

Furthermore, the energy [2] score function is proved to be more efficient in OOD detection, which quantifies the free energy function associated with each sample:

$$S_2(x; f) = -T \cdot \log \sum_j^C e^{y_j/T} \quad (7)$$

Both S_1 and S_2 exhibit large values on ID data and vice versa.

2) *Combination with feature rectification methods:* To further amplify the output difference between ID and OOD data, prior studies have explored the distribution of penultimate features and proposed feature rectification techniques, as OOD data is observed to exhibit larger feature values [4], [5]. However, our experimental findings indicate that applying these methods directly to our reduced gradients yields inferior performance compared to output-based approaches. Based on the distribution observation in Figure 3, we propose to exclusively rectify our low-dimensional gradients in certain dimensions and then feed them into the aforementioned linear network in (5). The overall process can be expressed as:

$$g \rightarrow \text{BN} \rightarrow \text{Clip}(g_d) \rightarrow \text{FC} \rightarrow y \quad (8)$$

where $g \in R^K$ and we denote $g_d \in R^d$ as the last- d dimensional vector of g . Different rectification approaches employ different Clip functions to truncate the values of gradients. For example, ReAct [4] method truncates activations above a threshold c to limit the effect of noises:

$$\text{Clip}(g_d) = \min(g_d, c)$$

where c a threshold that is determined based on the p -th percentile of g_d estimated on ID data. For example, when $p = 90$, it indicates that 90% percent of ID gradients are less than c . Apart from ReAct approach, BATS [5] method proposes to rectify extreme activations to the boundary values of typical sets with the guidance of batch normalization:

$$\text{Clip}(g_d) = \begin{cases} \mu + \lambda\delta & \text{if } g_d - \mu \geq \lambda\delta \\ \text{BN}(g_d) & \text{if } -\lambda\delta < g_d - \mu < \lambda\delta \\ \mu - \lambda\delta & \text{if } g_d - \mu \leq -\lambda\delta \end{cases}$$

where μ and δ are the learnable bias and weight of batch normalization layer, respectively, and λ is a hyperparameter. The typical set is defined as the interval $[\mu - \lambda\delta, \mu + \lambda\delta]$, within which all activations are constrained to reside. After the rectification of gradients, both the ReAct and BATS methods utilize the energy score function (Eq. (7)) to detect OOD samples.

3) *Combination with distance-based methods*: Features of ID data tend to cluster together and be away from those of OOD data; thus, previous works designed various distance measurements as score functions to detect OOD data. For our low-dimensional gradients, these methods should be equally effective since gradients share the same aggregation and separation properties as features, as shown in Figure 2. One typical measurement is the Mahalanobis distance [6] as follows:

$$S_3(x, f) = \max_c -(g - \hat{\mu}_c)^T \hat{\Sigma}^{-1} (g - \hat{\mu}_c) \quad (9)$$

where $\hat{\mu}_c$ and $\hat{\Sigma}$ are the empirical class mean and covariance of training samples. The Mahalanobis distance-based method imposes a class-conditional Gaussian distribution assumption about the underlying gradient space, while another distance-based approach named KNN [7] is more flexible and general without any distributional assumptions. It utilizes the Euclidean distance to the k -th nearest neighbor of training data as its score function, which can be expressed as follows:

$$S_4(x, f) = -\|g - \hat{g}_{(k)}\|_2 \quad (10)$$

Both S_3 and S_4 functions exhibit larger values on ID data and smaller values on OOD data since they take the negative value of the distance measurements.

4) *Ensemble of forward and backward information*: Drawing inspiration from the concept of integrating multiple sources of information to enhance detection performance, as demonstrated in [52], our work also tries to combine the scores obtained from the feature/output space with those derived from our reduced gradients. The algorithm for this combination is mathematically expressed as follows:

$$S_5(x, f) = S_f(x, f) + \alpha * S_b(x, f) \quad (11)$$

where α is the weight coefficient to ensure that S_f and $\alpha * S_b$ are of similar magnitude. In this paper, we set α as 1 in our experiments.

IV. EXPERIMENTS

In this section, we conduct a comparative analysis of the performance attained by employing gradients and features independently across six distinct detection methods. The analysis is performed on two widely recognized benchmark datasets, namely CIFAR10 [23] and ImageNet [24]. Additionally, we evaluate another three advanced detection approaches to validate our superior performance in OOD detection. Moreover, we assess the detection performance of utilizing the combined information from both forward and backward sources, which further reduces FPR95 and improves AUROC. At the end of this section, we investigate the impact of reduced dimensionality on our detection performance as well as the influence of various hyperparameters in the underlying methods. Through a comprehensive series of experiments, we provide compelling evidence for the effectiveness of employing low-dimensional gradients in OOD detection, thereby offering novel insights for future research endeavors. The detailed experimental configurations and settings are presented below.

OOD Datasets We evaluate our method on two popular benchmarks: CIFAR10 [23] and ImageNet [24]. When using CIFAR10 as ID data, we consider four OOD datasets as they are routinely used in literature: Textures [53], SVHN [54], LSUN-C [55], and iSUN [56]. As for the evaluation on ImageNet, we choose four commonly used OOD datasets that are subsets of: iNaturalist [57], SUN [58], Places [59], and Texture [53] with non-overlapping categories *w.r.t.* ImageNet.

Evaluation Metrics Two classical metrics are reported in this paper: 1) FPR95: the false positive rate of OOD samples when the true positive rate of ID samples is at 95%. 2) AUROC: the area under the receiver operating characteristic curve. The smaller the FPR95 and the higher the AUROC, the better the performance.

Model and Hyper-parameters In the case of CIFAR10, we adopt the ResNet18 architecture as our base model. We train it using the SGD algorithm with weight decay 0.0005, momentum 0.9, cosine schedule, initial learning rate 0.1, label smoothing 0.1, epoch 200, and batch size 128. The clean test accuracy is 96.39%. Regrading the ImageNet dataset, we use the pre-trained ResNet50 model in Pytorch [60], and the top-1 test accuracy is 76.13%. The pivotal hyper-parameter of our low-dimensional gradient is the reduced dimensionality, denoted as K . In our experiment, we set $K = 200$ for CIFAR10 and $K = 1000$ for ImageNet. We extract the principal subspace using PCA on CIFAR10 and average gradients on ImageNet.

Baseline Methods In this paper, we apply gradients and features separately within six different detection methods, including two output-based methods, namely MSP [1] and Energy [2], two feature rectification methods, namely ReAct [4] and BATS [5], and two distance-based methods, namely Mahalanobias [6] and KNN [7]. Additionally, we validate the superiority of our proposed approach by comparing

it with three other advanced detection methods, namely ODIN [3], GradNorm [9], and Vim [52]. Notably, all of the aforementioned approaches employ pre-trained networks in a post-hoc manner.

A. Evaluation on Large-scale ImageNet Benchmark

We first evaluate our method on the large-scale ImageNet benchmark, which poses significant challenges due to the substantial volume of training data and model parameters. The comparison results are presented in Table II, where we evaluate six different detection methods using either features or our low-dimensional gradients as inputs. To control our computational overhead, we randomly select 50000 training samples as the training dataset for our detection algorithms. We train the linear network in Eq.(5) with 0.01 learning rate, 512 batch size, and 3 epochs, achieving a test accuracy of 74.24%. For ReAct and BATS, we choose to truncate the last-50 dimensions of the 1000-dimensional gradients with $p = 0.7$ and $\lambda = 0.1$. Regarding the KNN method, we set $K = 10$ for both forward and backward embeddings.

It is worth noticing that our reduced gradients integrated with the simplest detection algorithm MSP achieve a surprisingly remarkable performance with FPR95 of 32.38% and AUROC of 91.87%, reducing the FPR95 by 32.38% and improving the AUROC by 9.05% compared to the original MSP. Furthermore, our gradients combined with the ReAct method achieve SOTA performance with FPR95 of 23.03% and AUROC of 95.45%, surpassing the best baseline by 7.67% in FPR95 and 2.15% in AUROC.

Our method achieves impeccable performance on the Places OOD dataset, which implies a significant disparity in the gradient space between the ImageNet and Places datasets. To gain further insight into this disparity, we randomly choose an OOD sample in the Places dataset and an ID sample in the ImageNet dataset and analyze the density distribution of their forward features and reduced gradients. The result presented in Figure 4 demonstrates that their distinctions are marginal in the feature space but pronounced in the gradient space, which aligns with the performance we achieve on the Places dataset.

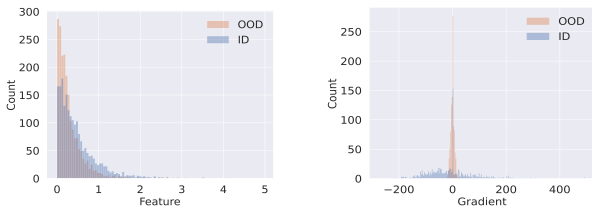


Fig. 4. Density distribution of features (left) and low-dimensional gradients (right) of two samples (one is OOD data from Places and the other is ID data from ImageNet). We can observe that the distinction between the two samples is marginal in the feature space but significant in the gradient space.

B. Evaluation on CIFAR10 Benchmark

To further demonstrate the effectiveness of our low-dimensional gradients, we also evaluate our method on the

CIFAR10 benchmark. The comparison results are presented in Table III. The hyper-parameters of baseline methods are set to the recommended values, i.e., $T = 1$ for Energy, $p = 0.9$ for ReAct, $\lambda = 0.1$ for BATS, and $K = 5$ for KNN. The Mahalanobis method we tested solely relies on the original distance formulation in Eq.(9) without incorporating any input pre-processing techniques or feature ensemble approaches. Thus, its performance is expected to be inferior to what has been reported in previous works where such enhancements were employed. Comparing all the results, our proposed gradients integrated with the KNN [7] method demonstrate superior performance, achieving the smallest FPR95 of 21.55% and the highest AUROC of 96.33%.

C. Comparison with Other Methods

In addition to the aforementioned approaches, there are other detection algorithms, such as ODIN [3], GradNorm [9], and Vim [52], that demonstrate outstanding performance but are not suitable for integration with our low-dimensional gradients. In this section, we compare our method with these algorithms to demonstrate our superior performance in OOD detection.

ODIN is an output-based method that incorporates the gradient of inputs as a data enhancement mechanism to obtain good detection performance. However, due to the fact that our low-dimensional gradients are not normalized to a scale of 0-1, it is difficult to determine an appropriate enhancement hyper-parameter. Hence, we do not combine ODIN with our reduced gradients.

GradNorm leverages the norm of parameter gradients as its scoring function to effectively identify OOD samples, exhibiting outstanding performance on the ImageNet benchmark dataset. Nevertheless, in our specific setting, where gradients are used as inputs to our linear network, GradNorm is not suitable.

Vim, a novel approach, capitalizes on the low-dimensionality of forward features and introduces a fusion strategy that combines the reconstruction error and energy score function as its detection function. However, the high dimensionality of gradients makes it computationally intensive to calculate the reconstruction error, thereby rendering this method inappropriate to apply to the gradients. Instead, we draw inspiration from the fusion concept and propose an ensemble strategy to detect OOD samples in Section IV-D.

The comparison results are presented in Figure 5. It can be observed that our method achieves comparable performance on CIFAR10 and superior performance on ImageNet. Our approach surpasses the best baseline method by 5.24% in terms of AUROC on the ImageNet benchmark.

D. Ensemble of forward and backward information

To further improve our detection performance, we explore strategies for integrating forward and backward information, as depicted in Eq.(11). We select the best-performing baseline method using our reduced gradients to conduct this ensemble approach. The experimental results are presented in Table IV, revealing the effectiveness of information ensemble in both

Table II. Results on ImageNet. Six different methods are evaluated respectively using forward features and backward gradients. The best result is in bold.

Methods	Embedding	iNaturalist		SUN		Places		Texture		Average	
		FPR95 ↓	AUROC ↑	FPR95 ↓	AUROC ↑	FPR95 ↓	AUROC ↑	FPR95 ↓	AUROC ↑	FPR95 ↓	AUROC ↑
MSP [1]	Feature	52.77	88.42	68.58	81.75	71.57	80.63	66.13	80.46	64.76	82.82
	Gradient	42.20	90.05	67.82	81.45	0.00	99.99	19.50	95.98	32.38	91.87
Energy [2]	Feature	53.93	90.59	58.27	86.73	65.40	84.13	52.29	86.73	57.47	87.05
	Gradient	28.79	93.39	67.52	82.26	0.00	100.00	15.28	96.70	27.90	93.09
ReAct [4]	Feature	19.49	96.40	24.07	94.40	33.48	91.92	45.74	90.47	30.70	93.30
	Gradient	19.87	95.77	45.34	90.52	0.00	100.00	26.90	95.50	23.03	95.45
BATS [5]	Feature	54.12	90.59	58.31	86.74	65.39	84.14	52.38	86.70	57.55	87.04
	Gradient	20.23	95.69	45.40	90.53	0.00	100.00	28.05	95.38	23.42	95.40
Maha [6]	Feature	93.70	65.81	97.56	49.91	97.63	49.44	37.13	91.18	81.51	64.09
	Gradient	95.41	47.93	96.88	52.66	100.00	37.87	56.90	58.78	87.30	49.31
KNN [7]	Feature	63.85	85.40	70.46	81.63	76.27	77.52	14.63	96.49	56.30	85.26
	Gradient	42.76	91.20	86.98	66.92	33.06	94.94	10.90	97.30	43.43	87.59

Table III. Comparison with six baseline methods on CIFAR10. Results are averaged across all OOD datasets. The best result is in bold.

Methods	MSP	Energy	ReAct	BATS	Maha	KNN	Ours
FPR95↓	33.08	29.47	36.46	21.66	22.27	27.59	21.55
AUROC↑	90.06	89.40	83.34	96.21	96.31	95.84	96.33

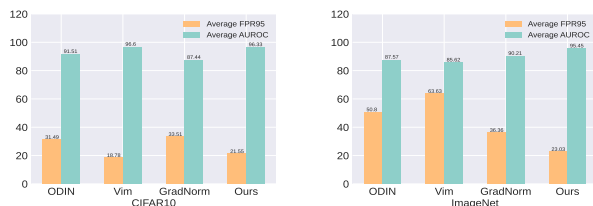


Fig. 5. Comparison with ODIN [3], GradNorm [9] and Vim [52] methods on CIFAR10 (left) and ImageNet (right).

CIFAR10 and ImageNet datasets. Particularly noteworthy is the further improvement in our performance on the ImageNet dataset, achieving an FPR95 of 19.55% and an AUROC of 96.12%.

Table IV. Detection performance with the ensemble of forward and backward information on CIFAR10 and ImageNet.

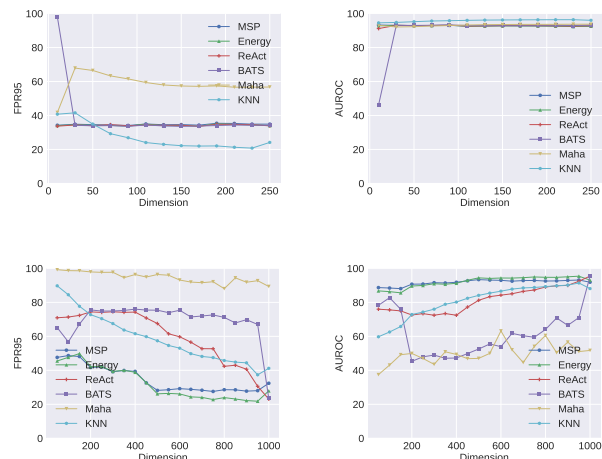
Dataset	Method	Metric	Embedding		
			Forward	Backward	Ensemble
CIFAR10	KNN	FPR95↓	27.59	21.55	20.24
		AUROC↑	95.84	96.33	96.79
ImageNet	ReAct	FPR95↓	30.70	23.03	19.55
		AUROC↑	93.30	95.45	96.12

E. Hyper-parameter study

In this section, we provide further analysis about the influence of hyper-parameters on our detection performance to demonstrate the stability of our approach. Specifically, we study the influence of the reduced dimension K on our detection performance. Besides, since our reduced gradients

are applied in different methods, we also investigate how the hyper-parameters in these methods impact our detection performance.

Effect of K In Figure 6, we systematically analyze the effect of K on six baseline methods. We vary the number of $K = \{10, 30, 50, 70, 90, 110, 130, 150, 170, 190, 210, 230, 250\}$ for CIFAR10 and $K = \{50, 100, 150, 200, 250, 300, 350, 400, 450, 500, 550, 600, 650, 700, 750, 800, 850, 900, 950, 1000\}$ for ImageNet. Our analysis reveals that the performance of our gradient-based methods improves as the dimension K increases, both for the CIFAR10 and ImageNet datasets. Notably, the FPR95 of the KNN method reaches its lowest value when $K = 230$ and exhibits a slight increase when $K = 250$. This observation aligns with the ratio analysis presented in Appendix A, where we observe that the first 230 principal components account for nearly 100% of the total variance. Intuitively, the optimal reduction dimension should be closely related to the principal component dimension of the gradients in the training data, which is consistent with our experimental results.

Fig. 6. The influence of the reduced dimension K on our detection performance across six baseline methods on CIFAR10 (top) and ImageNet (bottom).

Effect of Hyper-parameters in Baseline Methods We analyze how the following hyper-parameters influence our detection performance on their corresponding methods:

- The temperature T in Energy [2]
- The percent p in ReAct [4]
- The tuning parameter λ in BATS [5]
- The sort k in KNN [7]

Our experiments are conducted on ImageNet with a fixed reduced dimension of $K = 1000$. The results are presented in Figure 7. For the BATS and KNN methods, we observe that our performance remains stable with the change of hyper-parameters. In the case of the Energy method, the performance deteriorates with an increase in temperature, aligning with the observation in the original Energy [2] paper. Regarding the ReAct method, we observe a notable performance improvement when the percent changes from 0.5 to 0.6, which is expected since the gradients of ID data undergo a substantial impact when p is small. These results provide valuable insights into the sensitivity and stability of our approach with respect to specific hyper-parameters in different baseline methods.

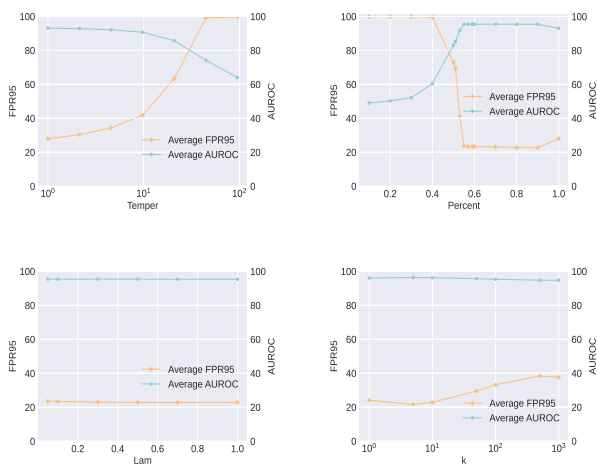


Fig. 7. The influence of hyper-parameters in baseline methods on our detection performance. Top left: the temperature T in Energy. Top right: the percent p in ReAct. Bottom left: the tuning parameter λ in BATS. Bottom right: the sort k in KNN.

V. LIMITATION

The extraction of our subspace requires some computational resources due to the involvement of intricate operations, such as gradient calculation and eigen decomposition of high dimensional matrix. Therefore, it is important to consider the available computing resources and optimize the implementation to ensure efficient execution of this process.

VI. CONCLUSION

This paper presents a pioneering study exploring the utilization of complete parameter gradient information for OOD detection. To solve the problem arising from the high dimensionality of gradients, we propose to conduct dimension reduction on gradients using our designated subspace, which comprises the principal components of gradients. With the

low-dimensional representations of gradients, we subsequently explore their integration with various detection algorithms. Our extensive experiments demonstrate that our low-dimensional gradients can notably improve performance across a wide range of detection tasks. We hope our work inspires further research on leveraging parameter gradients for OOD detection.

REFERENCES

- [1] D. Hendrycks and K. Gimpel, “A baseline for detecting misclassified and out-of-distribution examples in neural networks,” *arXiv preprint arXiv:1610.02136*, 2016.
- [2] W. Liu, X. Wang, J. Owens, and Y. Li, “Energy-based out-of-distribution detection,” *Advances in neural information processing systems*, vol. 33, pp. 21 464–21 475, 2020.
- [3] S. Liang, Y. Li, and R. Srikant, “Enhancing the reliability of out-of-distribution image detection in neural networks,” *arXiv preprint arXiv:1706.02690*, 2017.
- [4] Y. Sun, C. Guo, and Y. Li, “React: Out-of-distribution detection with rectified activations,” *Advances in Neural Information Processing Systems*, vol. 34, pp. 144–157, 2021.
- [5] Y. Zhu, Y. Chen, C. Xie, X. Li, R. Zhang, H. Xue, X. Tian, Y. Chen *et al.*, “Boosting out-of-distribution detection with typical features,” *arXiv preprint arXiv:2210.04200*, 2022.
- [6] K. Lee, K. Lee, H. Lee, and J. Shin, “A simple unified framework for detecting out-of-distribution samples and adversarial attacks,” *Advances in neural information processing systems*, vol. 31, 2018.
- [7] Y. Sun, Y. Ming, X. Zhu, and Y. Li, “Out-of-distribution detection with deep nearest neighbors,” in *International Conference on Machine Learning*. PMLR, 2022, pp. 20 827–20 840.
- [8] C. Igoe, Y. Chung, I. Char, and J. Schneider, “How useful are gradients for ood detection really?” *arXiv preprint arXiv:2205.10439*, 2022.
- [9] R. Huang, A. Geng, and Y. Li, “On the importance of gradients for detecting distributional shifts in the wild,” *Advances in Neural Information Processing Systems*, vol. 34, pp. 677–689, 2021.
- [10] J. Lee, C. Lehman, M. Prabhushankar, and G. AlRegib, “Probing the purview of neural networks via gradient analysis,” *IEEE Access*, vol. 11, pp. 32 716–32 732, 2023.
- [11] J. Sun, L. Yang, J. Zhang, F. Liu, M. Halappanavar, D. Fan, and Y. Cao, “Gradient-based novelty detection boosted by self-supervised binary classification,” in *Proceedings of the AAAI Conference on Artificial Intelligence*, vol. 36, no. 8, 2022, pp. 8370–8377.
- [12] J. Lee, M. Prabhushankar, and G. AlRegib, “Gradient-based adversarial and out-of-distribution detection,” *arXiv preprint arXiv:2206.08255*, 2022.
- [13] V. Szolnoky, V. Andersson, B. Kulcsar, and R. Jörnsten, “On the interpretability of regularisation for neural networks through model gradient similarity,” *Advances in Neural Information Processing Systems*, vol. 35, pp. 16 319–16 330, 2022.
- [14] A. Zimek, E. Schubert, and H.-P. Kriegel, “A survey on unsupervised outlier detection in high-dimensional numerical data,” *Statistical Analysis and Data Mining: The ASA Data Science Journal*, vol. 5, no. 5, pp. 363–387, 2012.
- [15] T. Li, L. Tan, Z. Huang, Q. Tao, Y. Liu, and X. Huang, “Low dimensional trajectory hypothesis is true: Dnns can be trained in tiny subspaces,” *IEEE Transactions on Pattern Analysis and Machine Intelligence*, vol. 45, no. 3, pp. 3411–3420, 2022.
- [16] E. J. Hu, Y. Shen, P. Wallis, Z. Allen-Zhu, Y. Li, S. Wang, L. Wang, and W. Chen, “Lora: Low-rank adaptation of large language models,” *arXiv preprint arXiv:2106.09685*, 2021.
- [17] A. Baratin, T. George, C. Laurent, R. D. Hjelm, G. Lajoie, P. Vincent, and S. Lacoste-Julien, “Implicit regularization via neural feature alignment,” in *International Conference on Artificial Intelligence and Statistics*. PMLR, 2021, pp. 2269–2277.
- [18] V. Pappayan, “Traces of class/cross-class structure pervade deep learning spectra,” *The Journal of Machine Learning Research*, vol. 21, no. 1, pp. 10 197–10 260, 2020.
- [19] A. Canatar, B. Bordelon, and C. Pehlevan, “Spectral bias and task-model alignment explain generalization in kernel regression and infinitely wide neural networks,” *Nature communications*, vol. 12, no. 1, p. 2914, 2021.
- [20] R. ZHANG, S. Zhai, E. Littwin, and J. M. Susskind, “Learning representation from neural fisher kernel with low-rank approximation,” in *International Conference on Learning Representations*, 2021.
- [21] S. Fort and S. Ganguli, “Emergent properties of the local geometry of neural loss landscapes,” *arXiv preprint arXiv:1910.05929*, 2019.

- [22] F. Mu, Y. Liang, and Y. Li, "Gradients as features for deep representation learning," in *International Conference on Learning Representations*, 2019.
- [23] A. Krizhevsky, G. Hinton *et al.*, "Learning multiple layers of features from tiny images," 2009.
- [24] J. Deng, W. Dong, R. Socher, L.-J. Li, K. Li, and L. Fei-Fei, "Imagenet: A large-scale hierarchical image database," in *2009 IEEE conference on computer vision and pattern recognition*. Ieee, 2009, pp. 248–255.
- [25] I. Kobyzev, S. J. Prince, and M. A. Brubaker, "Normalizing flows: An introduction and review of current methods," *IEEE transactions on pattern analysis and machine intelligence*, vol. 43, no. 11, pp. 3964–3979, 2020.
- [26] E. Zisselman and A. Tamar, "Deep residual flow for out of distribution detection," in *Proceedings of the IEEE/CVF Conference on Computer Vision and Pattern Recognition*, 2020, pp. 13 994–14 003.
- [27] D. P. Kingma and P. Dhariwal, "Glow: Generative flow with invertible 1x1 convolutions," *Advances in neural information processing systems*, vol. 31, 2018.
- [28] D. Jiang, S. Sun, and Y. Yu, "Revisiting flow generative models for out-of-distribution detection," in *International Conference on Learning Representations*, 2021.
- [29] H. Choi, E. Jang, and A. A. Alemi, "Waic, but why? generative ensembles for robust anomaly detection," *arXiv preprint arXiv:1810.01392*, 2018.
- [30] I. Ndiour, N. Ahuja, and O. Tickoo, "Out-of-distribution detection with subspace techniques and probabilistic modeling of features," *arXiv preprint arXiv:2012.04250*, 2020.
- [31] M. Cook, A. Zare, and P. Gader, "Outlier detection through null space analysis of neural networks," *arXiv preprint arXiv:2007.01263*, 2020.
- [32] J. Lust and A. P. Condurache, "Gran: An efficient gradient-norm based detector for adversarial and misclassified examples," *arXiv preprint arXiv:2004.09179*, 2020.
- [33] H. Wang, Z. Li, L. Feng, and W. Zhang, "Vim: Out-of-distribution with virtual-logit matching," in *Proceedings of the IEEE/CVF conference on computer vision and pattern recognition*, 2022, pp. 4921–4930.
- [34] K. Lee, H. Lee, K. Lee, and J. Shin, "Training confidence-calibrated classifiers for detecting out-of-distribution samples," *arXiv preprint arXiv:1711.09325*, 2017.
- [35] D. Hendrycks, M. Mazeika, and T. Dietterich, "Deep anomaly detection with outlier exposure," *arXiv preprint arXiv:1812.04606*, 2018.
- [36] H. Wei, R. Xie, H. Cheng, L. Feng, B. An, and Y. Li, "Mitigating neural network overconfidence with logit normalization," in *International Conference on Machine Learning*. PMLR, 2022, pp. 23 631–23 644.
- [37] Y. Ming, Y. Fan, and Y. Li, "Poem: Out-of-distribution detection with posterior sampling," in *International Conference on Machine Learning*. PMLR, 2022, pp. 15 650–15 665.
- [38] X. Du, X. Wang, G. Gozum, and Y. Li, "Unknown-aware object detection: Learning what you don't know from videos in the wild," in *Proceedings of the IEEE/CVF Conference on Computer Vision and Pattern Recognition*, 2022, pp. 13 678–13 688.
- [39] J. Katz-Samuels, J. B. Nakhleh, R. Nowak, and Y. Li, "Training ood detectors in their natural habitats," in *International Conference on Machine Learning*. PMLR, 2022, pp. 10 848–10 865.
- [40] T. Chen, S. Kornblith, M. Norouzi, and G. Hinton, "A simple framework for contrastive learning of visual representations," in *International conference on machine learning*. PMLR, 2020, pp. 1597–1607.
- [41] P. Khosla, P. Teterwak, C. Wang, A. Sarna, Y. Tian, P. Isola, A. Maschinot, C. Liu, and D. Krishnan, "Supervised contrastive learning," *Advances in neural information processing systems*, vol. 33, pp. 18 661–18 673, 2020.
- [42] Y. Ming, Y. Sun, O. Dia, and Y. Li, "Cider: Exploiting hyper-spherical embeddings for out-of-distribution detection," *arXiv preprint arXiv:2203.04450*, vol. 7, no. 10, 2022.
- [43] W. Grathwohl, K.-C. Wang, J.-H. Jacobsen, D. Duvenaud, M. Norouzi, and K. Swersky, "Your classifier is secretly an energy based model and you should treat it like one," *arXiv preprint arXiv:1912.03263*, 2019.
- [44] A. Jacot, F. Gabriel, and C. Hongler, "Neural tangent kernel: Convergence and generalization in neural networks," *Advances in neural information processing systems*, vol. 31, 2018.
- [45] S. Wold, K. Esbensen, and P. Geladi, "Principal component analysis," *Chemometrics and intelligent laboratory systems*, vol. 2, no. 1-3, pp. 37–52, 1987.
- [46] K.-J. Bathe, *Solution methods for large generalized eigenvalue problems in structural engineering*. National Technical Information Service, US Department of Commerce, 1971.
- [47] G. H. Golub and H. A. Van der Vorst, "Eigenvalue computation in the 20th century," *Journal of Computational and Applied Mathematics*, vol. 123, no. 1-2, pp. 35–65, 2000.
- [48] G. Charpiat, N. Girard, L. Felardos, and Y. Tarabalka, "Input similarity from the neural network perspective," *Advances in Neural Information Processing Systems*, vol. 32, 2019.
- [49] H. He and W. J. Su, "The local elasticity of neural networks," *arXiv preprint arXiv:1910.06943*, 2019.
- [50] S. Fort, P. K. Nowak, S. Jastrzebski, and S. Narayanan, "Stiffness: A new perspective on generalization in neural networks," *arXiv preprint arXiv:1901.09491*, 2019.
- [51] L. Van der Maaten and G. Hinton, "Visualizing data using t-sne." *Journal of machine learning research*, vol. 9, no. 11, 2008.
- [52] H. Wang, Z. Li, L. Feng, and W. Zhang, "Vim: Out-of-distribution with virtual-logit matching," in *Proceedings of the IEEE/CVF conference on computer vision and pattern recognition*, 2022, pp. 4921–4930.
- [53] M. Cimpoi, S. Maji, I. Kokkinos, S. Mohamed, and A. Vedaldi, "Describing textures in the wild," in *Proceedings of the IEEE conference on computer vision and pattern recognition*, 2014, pp. 3606–3613.
- [54] Y. Netzer, T. Wang, A. Coates, A. Bissacco, B. Wu, and A. Y. Ng, "Reading digits in natural images with unsupervised feature learning," 2011.
- [55] F. Yu, A. Seff, Y. Zhang, S. Song, T. Funkhouser, and J. Xiao, "Lsun: Construction of a large-scale image dataset using deep learning with humans in the loop," *arXiv preprint arXiv:1506.03365*, 2015.
- [56] P. Xu, K. A. Ehinger, Y. Zhang, A. Finkelstein, S. R. Kulkarni, and J. Xiao, "Turkergaze: Crowdsourcing saliency with webcam based eye tracking," *arXiv preprint arXiv:1504.06755*, 2015.
- [57] G. Van Horn, O. Mac Aodha, Y. Song, Y. Cui, C. Sun, A. Shepard, H. Adam, P. Perona, and S. Belongie, "The inaturalist species classification and detection dataset," in *Proceedings of the IEEE conference on computer vision and pattern recognition*, 2018, pp. 8769–8778.
- [58] J. Xiao, J. Hays, K. A. Ehinger, A. Oliva, and A. Torralba, "Sun database: Large-scale scene recognition from abbey to zoo," in *2010 IEEE computer society conference on computer vision and pattern recognition*. IEEE, 2010, pp. 3485–3492.
- [59] B. Zhou, A. Lapedriza, A. Khosla, A. Oliva, and A. Torralba, "Places: A 10 million image database for scene recognition," *IEEE transactions on pattern analysis and machine intelligence*, vol. 40, no. 6, pp. 1452–1464, 2017.
- [60] A. Paszke, S. Gross, S. Chintala, G. Chanan, E. Yang, Z. DeVito, Z. Lin, A. Desmaison, L. Antiga, and A. Lerer, "Automatic differentiation in pytorch," 2017.

APPENDIX A
EFFICIENT PCA FOR DNNs

Let us denote the gradient over the training dataset as $G \in \mathcal{R}^{n \times |\theta|}$, where n denotes the sample number and $|\theta|$ denotes the parameter number. To extract the low-dimensional subspace where the gradient principal components reside, we need to compute the top- K eigenvector of the gradient covariance $C = G^T G$. The main difficulties lie in two aspects: 1. The gradient matrix G is too large to calculate and save since both n and $|\theta|$ are enormous for modern DNNs. 2. Even if G and C are obtained, the eigen decomposition of C cannot be directly calculated because of its high dimensionality.

To solve the above problems, we employ the power iteration method [46], [47] to efficiently calculate the top- K eigenvectors of C , while ensuring computational feasibility. Noticing that the covariance matrix C is a dot product of G^T and G , each iteration step of the power method can be decomposed into two steps, as shown in Algorithm 2. And for each decomposed step, there exist efficient implementations in Pytorch [60] called Jacobian Vector Product (JVP) and Vector Jacobian Product (VJP), respectively, calculated at the same order of computational costs of one vanilla backward-pass and forward-pass of DNNs. Specific algorithms are shown in Algorithm 3 and Algorithm 4, where we integrate dataloaders into the algorithm. With this practical subspace extraction algorithm, we can obtain a low-dimensional subspace denoted by $v \in \mathcal{R}^{|\theta| \times K}$ that encompasses the principal components of gradients.

Algorithm 2 Power Iteration Method

Input: covariance matrix $C = G^T G \in \mathcal{R}^{|\theta| \times |\theta|}$, iteration step T , dimension number K

Output: top- K eigenvectors of C

- 1: **Draw random vector** $v \in \mathcal{R}^{|\theta| \times K}$
 - 2: **Schmidt orthogonalization of** v
 - 3: **for** $i = 1$ to T **do**
 - 4: $v \leftarrow Gv$ $\triangleright v = Gv \in \mathcal{R}^{n \times K}$
 - 5: $v \leftarrow G^T v$ $\triangleright v = G^T v \in \mathcal{R}^{|\theta| \times K}$
 - 6: **Schmidt orthogonalization of** v
 - 7: **end for**
 - 8: **return** v
-

Algorithm 3 Efficient Calculation of Gv

Input: vector $v \in \mathcal{R}^{|\theta| \times K}$, model f_θ , training dataloader D , mean matrix \mathcal{M} , variance matrix \mathcal{I}

Output: Gv

- 1: $v \leftarrow (\text{diag}(\mathcal{I})^{-\frac{1}{2}})v$
 - 2: $v_{out} \leftarrow []$
 - 3: **for** x in D **do**
 - 4: $a \leftarrow \text{functorch.jvp}(f_\theta, x, v) - \mathcal{M}v$
 $\triangleright a \in \mathcal{R}^{b \times K}, b: \text{batch size}$
 - 5: $v_{out} \leftarrow [a, v_{out}]$
 - 6: **end for**
 - 7: **return** v_{out}
-

Figure 8a shows the magnitude of the eigenvalues of the gradient covariance matrix calculated by our algorithm. It

Algorithm 4 Efficient Calculation of $G^T v$

Input: vector $v \in \mathcal{R}^{n \times K}$, model f_θ , training dataloader D , mean matrix \mathcal{M} , variance matrix \mathcal{I}

Output: $G^T v$

- 1: $v_{out} \leftarrow 0, j \leftarrow 0$
 - 2: **for** x in D **do**
 - 3: $v_t \leftarrow v[j : j + b]$ $\triangleright v_t \in \mathcal{R}^{b \times K}, b: \text{batch size}$
 - 4: $a \leftarrow \text{functorch.vjvp}(f_\theta, x, v_t)$
 - 5: $v_{out} \leftarrow v_{out} + a$
 - 6: $j \leftarrow j + b$
 - 7: **end for**
 - 8: $s \leftarrow \{\sum_i v[i, j]\}$ $\triangleright s \in \mathcal{R}^K$
 - 9: Expand the dimension of s to $\mathcal{R}^{|\theta| \times K}$
 - 10: $v_{out} \leftarrow (\text{diag}(\mathcal{I})^{-\frac{1}{2}})(v_{out} - \mathcal{M}s)$
 - 11: **return** v_{out}
-

can be observed that the eigenvalues tend to be concentrated within the initial 200 dimensions, with subsequent eigenvalues abruptly diminishing to zero. Additionally, we present Figure 8b, which illustrates the explained variance ratio as a function of the number of components. The results reveal that the top-200 principal components account for approximately 90% of the total variance. The above findings provide empirical validation for the low-dimensional nature of gradients.

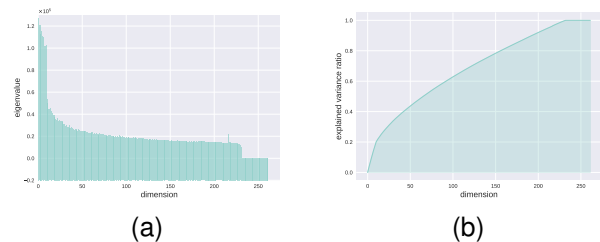


Fig. 8. (a): The magnitude of eigenvalues of the gradient covariance matrix; (b): The explained variance ratio as a function of the number of components. The results are derived from a well-trained ResNet18 model on CIFAR10.

APPENDIX B
GRADIENT DIRECTIONAL SIMILARITY

We examine the cosine similarity between the parameter gradient of a sample and its corresponding class-mean gradient on both the CIFAR10 and ImageNet datasets. In a high-dimensional space, the cosine similarity between two random vectors tends to approach zero, as verified in [14]. However, the average cosine similarity values presented in Table V are significantly higher than zero, which implies that gradients of samples belonging to the same class tend to align in similar directions.

Table V. The cosine similarity between the parameter gradient of a sample and its corresponding class-mean gradient. We report the average value, respectively, on the training and test datasets.

Dataset	Training Set	Test Set
CIFAR10	0.59	0.47
ImageNet	0.51	0.45